Dip Angle Effect on the Main Roof First Fracture and Instability in a Fully-mechanized Workface of Steeply Dipping Coal Seams

Zhen Wei
Anhui University of Science and technology https://orcid.org/0000-0003-1972-7456
Ke Yang (keyang2003@163.com)
Anhui University of Science and technology
Lou Xiao Chi
Anhui University of Science and Technology
Xin Yuan Zhao
Anhui University of Science and Technology
Xin Lv
Anhui University of Science and Technology

Research

Keywords: Steeply dipping workface, Dip angle, Main roof, First fracture, Support resistance

Posted Date: October 19th, 2020

DOI: https://doi.org/10.21203/rs.3.rs-92211/v1

Version of Record: A version of this preprint was published at Shock and Vibration on February 23rd, 2021. See the published version at https://doi.org/10.1155/2021/5557107.

Dip angle effect on the main roof first fracture and instability in a fully-mechanized workface of steeply dipping coal seams

Zhen Wei[1,3]· Ke Yang[1,2,3]· Xiaolou Chi[1,3] ·Xinyuan· Zhao[1,3]· Xin Lv[1,3]

Abstract The study of fracture and instability mechanism of the main roof in steeply dipping coal seams (SDCS) workface is crucial to the proper choice of support type and control of stability of surrounding rock, as well as the safe and effective mining in the coal seam. Based on the established SDCS main roof model, this study derived the stress distribution in the main roof under linear load, analyzed the dip angle effect associated with the evolving stress of SDCS workface, and elaborated the sequential characteristics of the ground pressure mechanism. Besides, an inclined unstable structure model of the main roof based on deformation, fracturing, and rotating of the main roof in the SDCS workface was also proposed here, which explained the impacts of overburden rock's key parameters on sliding and rotatory instability of rock mass. In light of the analysis of the movement rule of overburden rock and loading condition of support, it is found that, when the roof and floor in the workface are stable, the critical support resistance with the absence of sliding and rotating increases as the dip angle of coal seam increases, the roof is in the state of discontinuous movement due to its self-weight and overburden pressure. Support is affected by the discontinuous movement and moved along with the roof. The results of this study can be of theoretical reference to the control of SDCS.

Keywords Steeply dipping workface; Dip angle; Main roof; First fracture; Support resistance

1 Introduction

With a gradual reduction of coal resources and growing mining intensity, mining under complicated conditions has been increasing in recent years (Wu et al. 2014). In particular, steeply dipping coal seams (SDCS) are regarded as difficult for mining (Ye et al. 2017; Wu et al. 2010; Tu et al. 2019). However, with the development of fully-mechanized mining theories, advancing research of equipment, and improved management in the workface, SDCS with shallow depth has gradually become the main coal seam in western China's mining areas. For example, the Sichuan Coal Industry Group Ltd. has succeeded in the trial mining in the Lvshuidong coal seam with a dip angle of 70°. The rock pressure pattern in the SDCS workface is influenced by a dip angle, which results in a significant difference from coal seam with a low dip angle during mining (Kang et al. 2002; Shi et al. 2018). The available pressure control and technology theories focused on horizontal coal seams and coal seams with a shallow dip

✉ Ke Yang
Keyang2003@163.com

1 State Key Laboratory of Mining Response and Disaster Prevention and Control in Deep Coal Mines, Anhui University of Science and Technology, Huainan 232001, Anhui, China

2 Institute of Energy, Hefei Comprehensive National Science Center, Hefei 230031, Anhui, China

3 Key Laboratory of Mining Coal Safety and Construction Efficiency of Anhui Province and Ministry of Education, Anhui University of Science and Technology, Huainan 232001, Anhui, China

angle cannot guide the safe and efficient mining in SDCS. At present, roof falling, flying gangue in workface, and hydraulic support sliding are the major disasters in SDCS mining (Shan et al. 2020; Hu et al. 2017) and are all directly related to roof stability. Therefore, the study of roof failure and movement is the prerequisite for safe and efficient mining in SDCS (Zhang et al. 2018; Das et al. 2017).

Numerous field test results proved that mining in SDCS caused roof weighting in different zones in the workface, and the ground pressure became abnormal. Studies of fracturing in different zones in the roof of the SDCS workface were conducted by different researchers and were focused on the failure, migration, and evolution law of the workface roof (Wang et al. 2015b). Several studies performed the analysis of the fracturing pattern of the main roof in the workface and the relationship between the support-surrounding rock (Jiang et al. 2014). Establish a mechanical model of stope roof based on elastic theory, analyze the evolution characteristics of basic roof fracture, and obtain fracture forms in different periods (Wang et al. 2016; Cui et al. 2019). Based on the hinged rock block model, the limit position of the rotation instability of the hinged structure is studied, and the unique instability mode of the shallow-buried thin bedrock roof and the method for determining the working resistance of the support are proposed (Wang et al. 2015a). Based on the theoretical model of inclined coal seam stope, the stress distribution characteristics and fracture mechanism of basic roof strata during mining are analyzed (Zhang et al. 2010; Yang et al. 2013).

Based on beam and plate models, numerous researchers systematically investigated the fracture and evolution law of a roof in a fully-mechanized workface, improved the understanding of the main roof's first fracture, and refined the surrounding rock control theory. However, due to the complex characteristics of mines' geological conditions, it is difficult to fully and accurately reflect the fracture evolution law of the roof during mining in the coal seam and further study the dip angle effect on the kinematic movement law of overburden rock is highly demanded. Therefore, based on available findings, this study utilized a theoretical analysis method and elaborated a mechanical model of the main roof in SDCS to investigate the effect of dip angle on the first fracture of the main roof in a fully-mechanized workface. Thus, it determined the key factors controlling the surrounding rock stability. The results in this study provide theoretical reference for the effective preventive measures in mining.

2 Assumptions of the main roof mechanical model

According to the assumption of a thin plate (or a slender body) in the elasticity theory (Yang et al. 2013), an elastic plate can be treated as a thin plate if the ratio between its thickness h and length of its shortest side l satisfies the following conditions:

$$\left(\frac{1}{100}:\ \frac{1}{80}\right)\le\frac{h}{l}\le\left(\frac{1}{8}:\ \frac{1}{5}\right) \tag{1}$$

Below the first-fracture mining pressure in the longwall workface in SDCS is reached, the main roof can be regarded as a thin plate since its thickness and length satisfy the above equation.

Hard hanging roof zone appears in the goaf rear area after mining in the workface. Usually, the narrow coal pillar side and fault side are treated as simple boundaries. The solid coal side is treated as a clamped boundary (Jiang et al. 2014), where deflection and rotation are zero.

3. Rule of the first fracture of the main roof

3.1 Basic equations of thin plate

As mining advances from the open-off cut, the main roof's exposed area gradually increases, and fracturing happens when the stress reaches the stratum's ultimate strength. The main roof in the SDCS workface is supported by integrated coal before fracturing. Since the coal seam's dip angle is relatively large, the false and immediate roofs fall to the bottom of goaf as mining proceeds. Therefore, a mechanical model of the main roof in SDCS, as shown in Fig. 1, was elaborated in this study. Herein, the dip angle of the coal seam is α, the x-axis is directed along the workface strike with a length of a, the y-axis is along the workface dip with a length of b, and the z-axis is normal to the roof and has positive downward direction.

Due to the impact of dip angle, the load from overburden rock that acts on the roof can be simplified as P(y) that linearly changes along the dip (i.e., positive axis), which is expressed as:

$$P(y)=P_0-\gamma y\sin\alpha \tag{2}$$

where γ is the average unit weight of the overburden rock and P0 is the overburden load in the roadway of workface. The later value, P_0 , is decomposed into the force

perpendicular to the roof denoted by $P_1 = P(y)\cos\alpha$ and the force parallel to the roof denoted by $P_2 = P(y)\sin\alpha$. Since the latter force component P_2 is much smaller than P_1 within the dip angle range under study, its effect is neglected, and the deflection function of the main roof under the linear overburden load is written as:

$$\omega_1(x,y)=A_1\left(y+\frac{b}{4}\right)\sin^2(\frac{\pi x}{a})\sin^2(\frac{\pi y}{b}) \quad (3)$$

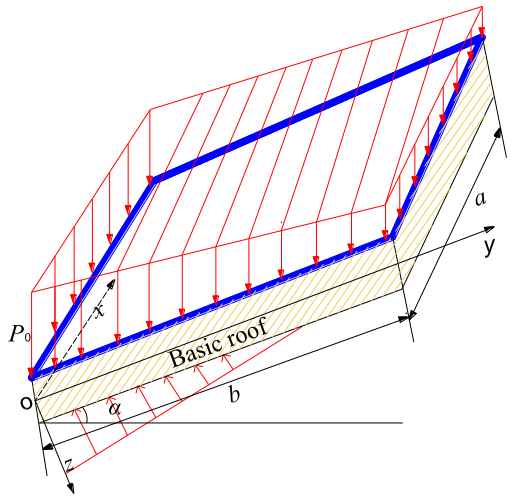

Fig. 1. Mechanical model of the main roof in SDCS

The following boundary conditions have to be satisfied:

$$(\omega_1)_{x=0,a}=0 \qquad (\omega_1)_{y=0,b}=0$$

$$\left(\frac{\partial\omega_1}{\partial x}\right)_{x=0,a}=0 \qquad \left(\frac{\partial\omega_1}{\partial y}\right)_{y=0,b}=0 \quad (4)$$

According to the principle of minimum potential energy (Yang et al. 2013), the total potential energy of a thin plate under the linear overburden load is:

$$E_P=\frac{D}{2}\iint\left\{\left(\frac{\partial^2\omega_1}{\partial x^2}+\frac{\partial^2\omega_1}{\partial y^2}\right)^2-2(1-\mu)\left[\frac{\partial^2\omega_1}{\partial x^2}\frac{\partial^2\omega_1}{\partial y^2}-(\frac{\partial^2\omega_1}{\partial x\partial y})^2\right]\right\}dxdy-\iint P_1\omega_1 dxdy \quad (5)$$

where P_1 is the overburden load perpendicular to the roof, ω_1 is the deflection function of the main roof under linear overburden load, and μ is Poisson's ratio.

Since $\frac{\partial E_P}{\partial A_1}=0$, the deflection function coefficient can be calculated by

$$A_1=\frac{\frac{3}{16}P_0\cos\alpha ab^2-\frac{11}{96}\gamma\sin\alpha\cos\alpha ab^3}{\frac{D(1-\mu)}{a}\mathrm{b}(\frac{3\pi^2}{8}+\frac{\pi^3}{10}-\frac{47\pi^4}{120})} \quad (6)$$

Substituting Eq (6) into Eq (3) yields the deflection function of the main roof with four fixed sides under the linear overburden load

$$\omega_1(x,y)=\left(\frac{3}{16}P_0\cos\alpha ab^2-\frac{11}{96}\gamma\sin\alpha\cos\alpha ab^3\right)\left(\mathrm{y}+\frac{b}{4}\right)\sin^2(\frac{\pi x}{a})\sin^2(\frac{\pi y}{b})/\left[\frac{D(1-\mu)}{a}\mathrm{b}(\frac{3\pi^2}{8}+\frac{\pi^3}{10}-\frac{47\pi^4}{120})\right] \quad (7)$$

where D is the bending stiffness of the thin plate, $D=\frac{Eh^3}{12(1-\mu^2)}$; E is the elastic modulus of the main roof; h is the main roof thickness.

Gangue filling in the goaf of SDCS is highly heterogeneous. Hence, the upper, middle, and bottom areas of the main roof have different stress states and kinematic movement patterns. It is assumed that falling gangue fills two-thirds of the total space of goaf of SDCS, the bottom area has good filling and is closer to the intact rock strength than the middle area, and the upper area has no filling, so a load of gangue filling on the main roof P_3 is derived as follows:

$$P_3=P_0-\frac{3yP_0}{2b}(0\le y\le\frac{2}{3}b) \quad (8)$$

According to the principle of minimum potential energy, the deflection function of the main roof under gangue filling is

$$\omega_2(x,y)=\frac{96a^2b^4P_0y}{D(1-\mu)\pi^3(535b^4+363a^2b^2+315a^4)}\sin^2(\frac{\pi x}{a})\sin^2(\frac{\pi y}{b}) \quad (9)$$

Using Eqs. (7) and (9) to derive $\omega=\omega_1-\omega_2$, one gets in the total deflection function of SDCS main roof under overburden pressure and gangue filling conditions.

3.2 Stress expression

Using the coefficient $A_2=\frac{96a^2b^4P_0y}{D(1-\mu)\pi^3(535b^4+363a^2b^2+315a^4)}$ and the relation between deflection and stress in the theory of thin elastic plate, stresses in the SDCS main roof can be derived as follows:

$$\sigma_x = -\frac{Ez(A_1 - A_2)}{1-\mu^2}\left[\left(\frac{b\pi^2}{2a^2}+\frac{2\pi^2 y}{a^2}\right)\cos\left(\frac{2\pi x}{a}\right)\sin^2\left(\frac{\pi y}{b}\right)+\frac{2\pi\mu}{b}\sin^2\left(\frac{\pi x}{a}\right)\sin\left(\frac{2\pi y}{b}\right)+\sin^2\left(\frac{\pi x}{a}\right)\cos\left(\frac{2\pi y}{b}\right)\left(\frac{2\pi^2\mu y}{b^2}+\frac{\pi^2\mu}{2b}\right)\right]$$

$$\sigma_y = -\frac{Ez(A_1 - A_2)}{1-\mu^2}\left[\frac{2\pi}{b}\sin^2\left(\frac{\pi x}{a}\right)\sin\left(\frac{2\pi y}{b}\right)+\sin^2\left(\frac{\pi x}{a}\right)\cos\left(\frac{2\pi y}{b}\right)\left(\frac{2\pi^2 y}{b^2}+\frac{\pi^2}{2b}\right)+\left(\frac{b\pi^2\mu}{2a^2}+\frac{2\pi^2\mu y}{a^2}\right)\cos\left(\frac{2\pi x}{a}\right)\sin^2\left(\frac{\pi y}{b}\right)\right] \quad (10)$$

$$\tau_{xy} = -\frac{Ez(A_1 - A_2)}{1+\mu}\left[\frac{\pi}{a}\sin^2\left(\frac{\pi y}{b}\right)\sin\left(\frac{2\pi x}{a}\right)+\left(\frac{\pi^2 y}{ab}+\frac{\pi}{4}\right)\sin\left(\frac{2\pi y}{b}\right)\sin\left(\frac{2\pi x}{a}\right)\right]$$

where $0 \le x \le a$, $0 \le y \le b$, and $-\frac{h}{2} \le z \le \frac{h}{2}$.

3.3 Stress distribution in the main roof

During mining in the coal seam, when the roof's maximum tensile stress exceeds its tensile strength σ_t, the tensile fracture will occur (Zhao et al. 2019). According to Eq.(10), the distributions of σ_x and σ_y in the bottom floor were obtained and depicted in Fig. 2.

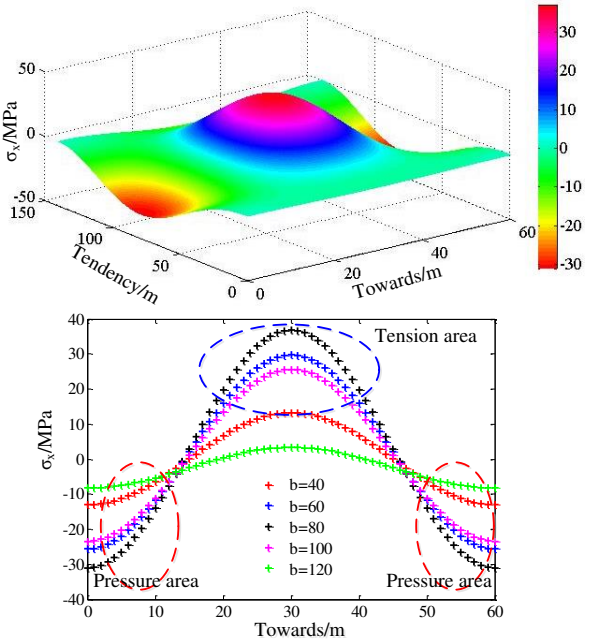

(a) σ_x

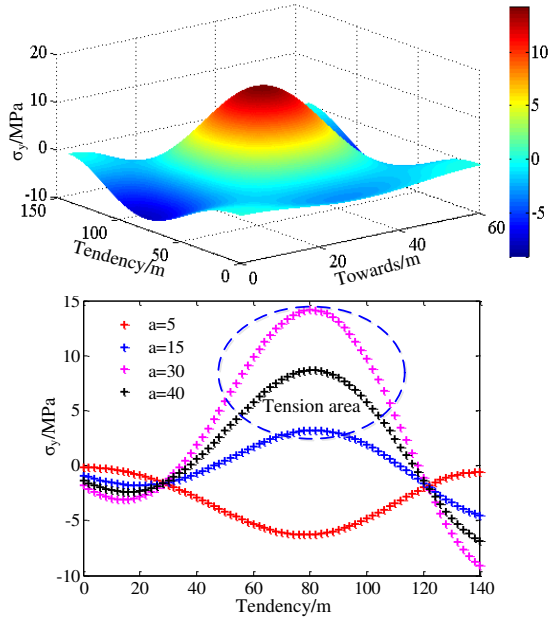

(b) σ_y

Fig. 2. Characteristics of σ_x and σ_y in the bottom floor of the thin plate

In Fig.2(a), where σ_x is the compressive stress ranging from 0 to 15 MPa and from 45 to 60 MPa. The tensile stress portion ranges from 15 to 45 MPa and is symmetrical along the advance direction of the workface. Meanwhile, in Fig.2(b), σ_y is the compressive stress ranging from 0 to 30 MPa and from 120 to 140 MPa. It keeps increasing the thin roof with the workface advance, while the upper area experiences compression → tension → compression, and shows asymmetry as a whole along the dip of workface.

While σ_x reaches its peak value at $x=\frac{a}{2}$ and y =0.56, σ_y reaches its peak value at $x=\frac{a}{2}$ and y =0.58 b . The maximum stress can be calculated as follows.

$$\sigma_{x\max}=-\frac{12Dz(A_1-A_2)}{h^3}\left[\frac{1.615\pi^2\mu+0.122\pi\mu}{b}-9.425\times10^{-4}\times\left(\frac{b\pi^2+2.24\pi^2}{2a^2}\right)\right] \quad (11)$$

$$\sigma_{y\max}=-\frac{12Dz(A_1-A_2)}{h^3}\left[\frac{1.656\pi^2+0.127\pi}{b}-1.01\times10^{-3}\times\left(\frac{b\mu\pi^2+2.32\mu\pi^2}{2a^2}\right)\right] \quad (12)$$

As observed, $\sigma_{x\max}>\sigma_{y\max}$. Hence, σ_x the main factor controlling the fracturing instability of the overburden rock, while the dip angle of the coal seam only changes the rock's tensile stress (i.e., the ultimate span of workface). When the maximum tensile stress reaches the tensile strength limit at a certain point in the thin rock plate, the tensile fracture occurs, and gradually thin rock plate evolves into spatial surrounding rock structure.

Current studies show that when the tensile stress exceeds the shear stress, while the latter exceeds the compressive stress ($\sigma_{tensile}<\sigma_{shear}<\sigma_{compressive}$), the tensile or shear failure is likely to take place in stratum, and the failure pattern is determined by its tension and shear strengths as well as the stress within the stratum (Yang et al. 2015). Therefore, the analysis of distributions of principal stress and shear stress on the main roof is of great significance. Relations between the roof stress components and principal stress, as well as shear stress, are described by the following equations.

$$\begin{matrix}\sigma_{\max}\\ \sigma_{\min}\end{matrix}=\frac{\sigma_x+\sigma_y}{2}\pm\sqrt{\frac{(\sigma_x-\sigma_y)^2}{2}+\tau_{xy}{}^2} \quad (13)$$

$$\tau_{\max}=\frac{\sigma_{\max}-\sigma_{\min}}{2} \quad (14)$$

Equations (13) and (14) determine the principal stresses $\sigma_{\max}$ and $\sigma_{\min}$, and shear stress $\tau_{\max}$ at any point in the thin floor where the four boundaries are fixed. The above stresses depend on the main roof's thickness h and length-to-width ratio, overburden pressure, and coal seam dip angle α. Hence, the overburden load P_0 above the roadway of the workface can be any load that satisfies $P_1\geq0$, which is $P_0\cos\alpha-\gamma y\sin\alpha\cos\alpha\geq0$. Here, P0=10MPa, Poisson's ratio of the main roof μ =0.25, the main roof elastic modulus E =30GPa, the main roof thickness h =6m, coal seam dip angle α =40°, strike length of the main roof a =60m, and dip length b =140m. The principal stress distribution in the thin main roof is shown in Fig. 3.

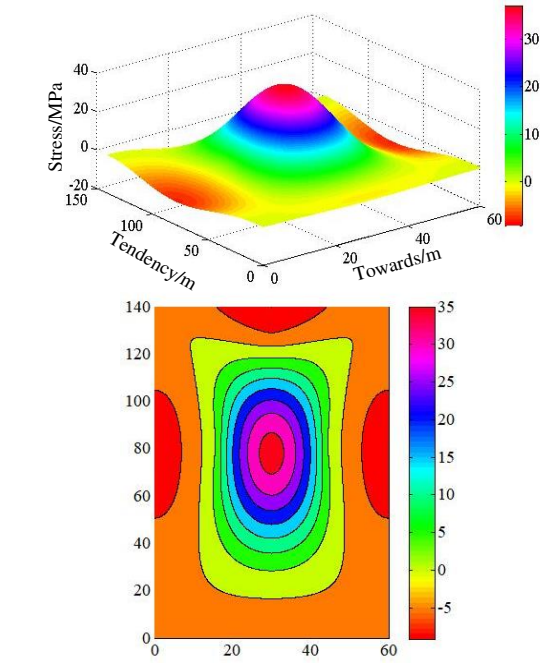

(a) $\sigma_{\max}$

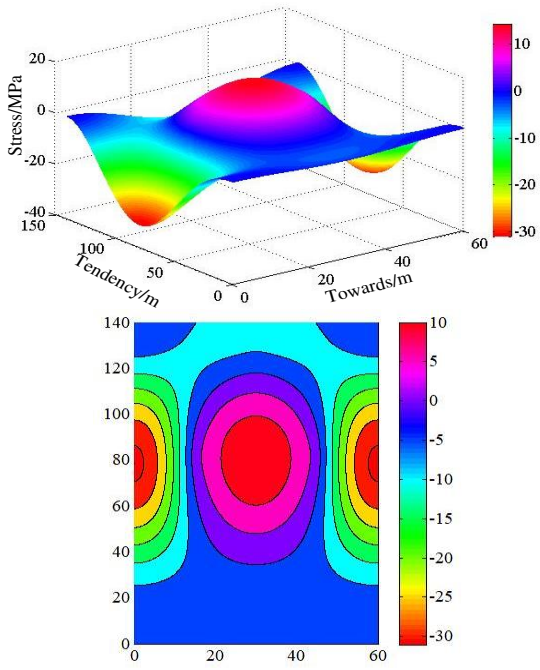

(b) $\sigma_{\min}$

Fig.3. Neophogram of the principal stress in the main roof

It can be seen from Fig. 3 that the principal stresses σ_{max} and σ_{min} in the upper-middle zone of the main roof in SDCS longwall workface are positive, indicating that the top roof ($z=-\frac{h}{2}$) is compressed and the bottom roof is under tension. Meanwhile, σ_{max} and σ_{min} in the upper zone of upper boundary and left and right zones of vertical boundaries in suspense zone are negative, implying that the top roof ($z=-\frac{h}{2}$) is under tension, and the bottom roof is under compression. It shows that the bottom roof is under compression at three boundaries and tension in the middle zone, while the top roof is under tension at three boundaries and compression in the middle zone.

The maximum shear stress distribution in the main roof with the same parameters is depicted in Fig. 4. The maximum shear stress τ_{max} occurs periodically in the upper-middle zone of the main roof in the SDCS longwall workface as mining is advancing, and it is large in the middle but small on both sides. Since rock has a very low tensile strength, failure is likely to occur in the bottom roof's upper-middle zone. Both sides of the long boundaries of the top roof, as well as the upper zone of the short boundary, and the failure in the middle zone of the bottom roof will develop toward the long boundaries.

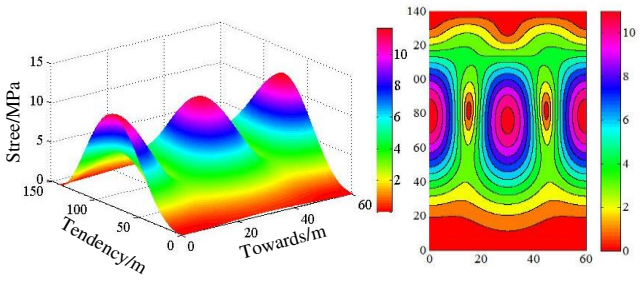

Fig. 4. Neophogram of maximum shear stress of the main roof

Using $\frac{\sigma_{max}}{\tau_{min}}=\eta$, the principal stresses σ_{max} and σ_{min} and the maximum shear stress τ_{max} in the main roof during the first weighing in coal seam with different dip angles were calculated, and the results are depicted in Fig. 4. Principal stresses σ_{max} and σ_{min} are non-linearly correlated with the dip angle α, principal stress decreases as the dip angle α increases, and σ_{max} reduces rapidly as dip angle increases in the range 30°~50°. This implies that the dip angle had a strong impact on the roof stress in this range. Stresses σ_{max} and σ_{min} gradually become stable as the dip angle increases in the range 50°~60°, meaning that the dip angle has a weak effect on the roof stress in this range. The maximum shear stress τ_{max} exhibits the same evolution trend as the dip angle increases. The principal stress variation rate is defined by η, which turns out to be constant, meaning that σ_{max} and σ_{min} have the same variation rates for the same dip angle increments.

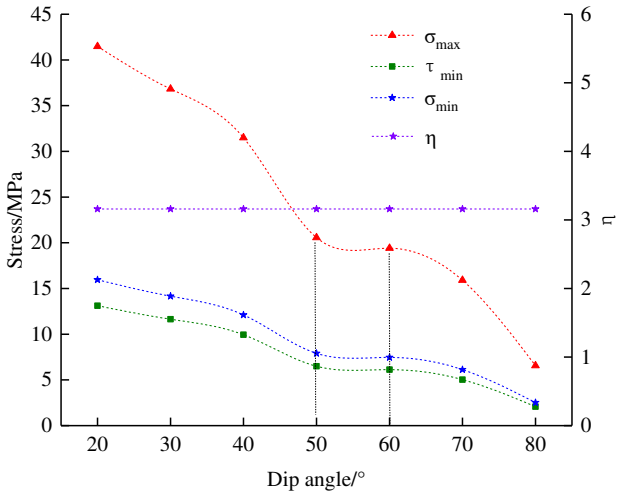

Fig. 5. Relationship between stresses in the thin stratum and the dip angle

4 Fracturing instability characteristics of the main roof

4.1 Slip instability of the main roof

Asymmetrical mechanical characteristics of the SDCS workface, as well as dip strata movements, are resulte d from the heterogeneous features of dip angle and g angue, and the lager the dip angle is, the more distin ct the asymmetrical features strata movement has (Hu et al. 2018).Strata movement undergoes “failure—fall ing—fracturing—settling—rotating” when exposed to c omplex stress state conditions.

As workface advances, the vertical and separation fractures occur in a certain range of overburden rock. The extrusion between rock blocks induces an asymmetrical hinged rock structure. It gradually develops into a macroscopic "shell" structure (Xie et al. 2009; Zhang et al. 2015; Xie et al. 2019). A typical rock block is subjected to the stress state shown in Fig. 6.

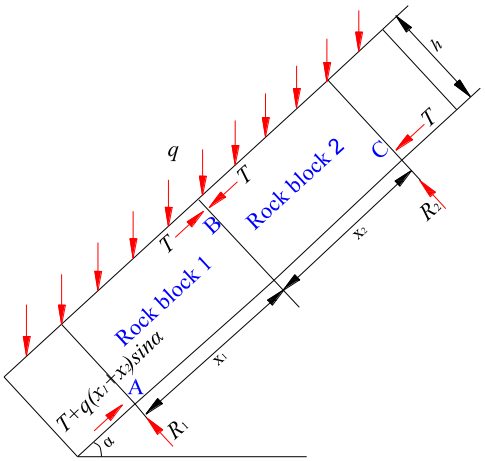

（a） stress characteristics of the whole model

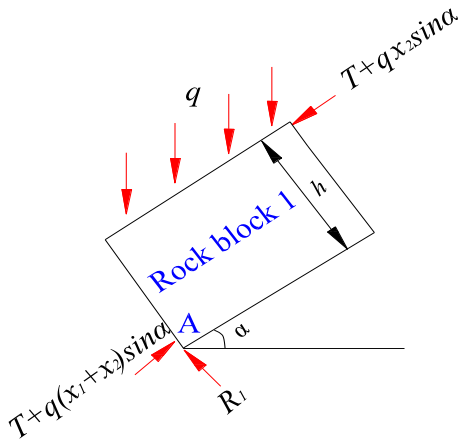

(b) stress characteristics of the rock block 1

Fig. 6. Mechanical model of the inclined fractured rock block

The hinged structure is framed into the Cartesian coordinate system and satisfies the following mechanical equilibrium equations:

$$\begin{cases} (R_1+R_2)-q(x_1+x_2)\cos\alpha=0 \\ \dfrac{qx_1^2}{2}\cos\alpha-\dfrac{qx_1h}{2}\sin\alpha-(T+qx_2\sin\alpha)h=0 \\ \dfrac{q(x_1+x_2)^2}{2}\cos\alpha-\dfrac{q(x_1+x_2)h}{2}\sin\alpha-R_2(x_1+x_2)=0 \end{cases} \quad (15)$$

Solving these equations, one can derive shear stresses R_1 and R_2 and the extrusion stress T

$$\begin{cases} R_1=\dfrac{q(x_1+x_2)\cos\alpha}{2}+\dfrac{qh\sin\alpha}{2} \\ R_2=\dfrac{q(x_1+x_2)\cos\alpha}{2}-\dfrac{qh\sin\alpha}{2} \\ T=\dfrac{qx_1^2\cos\alpha}{2h}-\dfrac{qx_1\cos\alpha}{2}-qx_2\sin\alpha \end{cases} \quad (16)$$

where h is the main roof thickness, α is the coal seam's dip angle, while x_1, and x_2 are the lengths of fractured rock blocks.

The slip instability occurs when the shear stress exceeds the extrusion stress in the rock block. Thus, the mechanical balance equation for the hinged structure should be satisfied to avoid slip instability, i.e.

$$\frac{(x_1+x_2)\cos\alpha+h\sin\alpha}{hx_1^2\cos\alpha-h^2x_1\cos\alpha-2h^2x_2\sin\alpha}\le\tan\varphi \quad (17)$$

where φ is the friction angle of the fractured rock block, which is usually taken as φ =38~45°, $\tan\varphi$ =0.8~1 (Zhou et al. 2019).

Lengths of hinged rock blocks are assumed to be the same, that is, $x_1=x_2$. The ratio of shear stress R to extrusion stress T in the hinged area is defined as a slip coefficient λ derived as

$$\lambda=\frac{2x\cos\alpha+h\sin\alpha}{hx^2\cos\alpha-h^2x\cos\alpha-2h^2x\sin\alpha} \quad (18)$$

When the ratio of the hinged rock block's length to the thickness of the main roof is constant, the slip coefficient changes with the dip angle ranging from 20º to 70º, and the relationship is depicted in Fig. 7.

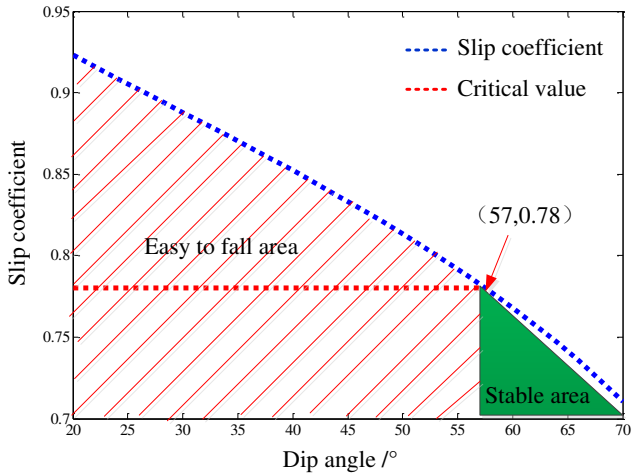

Fig. 7. Relationship between slip coefficient λ and dip angle α

Figure 7 shows that the fractured rock block's slip coefficient linearly decreases as the dip angle increases, indicating the larger dip angle provides a higher anti-sliding capacity of the rock block with a hinge structure, making sliding unlikely to occur. Taking the friction angle of the fractured rock block at 38°, we get $\tan\varphi$=0.78 as the critical sliding coefficient,< Thus, the green area in Fig. 7 is the stable area, indicating a critical dip angle of 57°.

At constant dip angle α values, the slip coefficient's evolution trend for the main roof thickness h and length l ranges of 5m < h < 15m and 10m < l < 30m is shown in Fig. 8.

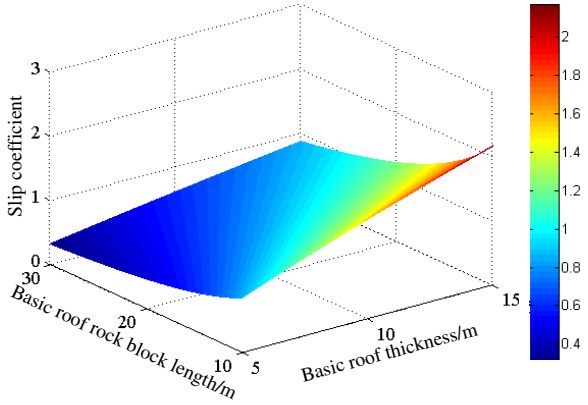

Fig. 8. Relationship between slip coefficient λ, main roof thickness h , and length x

It can be seen from Fig. 8 that the slip coefficient linearly increases as h and x increase. The greater thickness-to-length ratio *h/l* corresponds to a larger slip coefficient λ , indicating a high possibility of the roof slip instability. The greater the thickness of the main roof and the fractured rock block's length, the larger load support will have to bear when the roof is unstable, inducing high mining pressures.

4.2 Rotatory instability model of the main roof

Under the overburden stress, the hinge area of the rock block is bearing compressive force and is likely to experience plastic failure, thus accelerating the rotatory instability of the hinged structure (Wang et al. 2019; Sun et al. 2019). The rotatory instability model of fractured rock block is shown in Fig. 9.

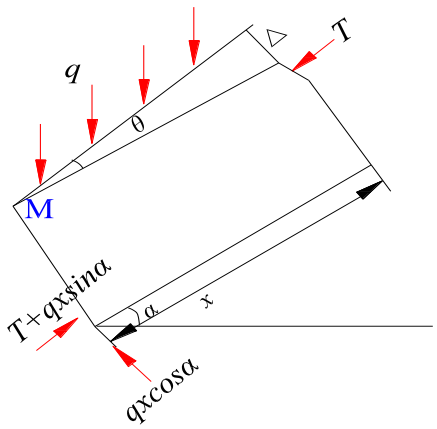

Fig. 9. Rotatory instability mechanical model of fractured rock block

When the hinged rock block is in the limit equilibrium, the sum of all moments is zero, i.e., $\sum M=0$. Then:

$$T\left(h-a-\Delta\right)=\frac{qx^2\cos\alpha-\left(h-a\right)qx\sin\alpha}{2} \tag{19}$$

where a is the width of the hinged area of the rock block in the main roof, θ is the angle of rotation of the fractured rock block, and x is the rock block length.

When a is relatively small, we get:

$$\begin{cases} 2a=h-x\sin\theta \\ \Delta=x\sin\theta \end{cases} \tag{20}$$

Combining Eq (19) and (20) gives

$$\frac{2qx^2\cos\alpha-qx\sin\alpha\left(h+x\sin\theta\right)}{2\left(h-x\sin\theta\right)} \tag{21}$$

According to the strength criterion for rocks, the hinged structure of the main roof has to satisfy the following condition if when rotatory instability is absent

$$\sigma_c\geq\sigma_p=\frac{2qx^2\cos\alpha-qx\sin\alpha\left(h+x\sin\theta\right)}{\left(h-x\sin\theta\right)^2} \tag{22}$$

where θ is the angle of rotation of the fractured rock block, σ_c is the fractured rock block's compressive strength, and σ_p is the extrusive strength between two adjacent rock blocks.

The rotatory coefficient ξ is defined as the ratio of extrusive strength of the fractured rock block σ_p to the compressive strength σ_c . Thus, the ultimate load q that the rock block can bear is

$$q=\frac{\xi\sigma_c\left(h-x\sin\theta\right)^2}{2x^2\cos\alpha-xh\sin\alpha-x^2\sin\alpha\sin\theta} \tag{23}$$

When the roof beam is fractured, the ultimate load q and tensile strength σ_t are related as follows:

$$q=\frac{\sigma_t}{6\kappa\left(\frac{x}{h}\right)^2} \tag{24}$$

where κ value depends on the boundary conditions of the hinged rock block. Combining Eqs. (23) and (24) yields the following formulas:

$$\begin{cases} \sin\theta=\frac{h}{x}-\left[\begin{array}{l}h^2\sigma_t\sin\alpha+\\ \sqrt{h^2\sigma_t^{\,2}\sin^2\alpha-48h^2\xi\kappa\sigma_c\sigma_t\left(hx\sin\alpha-x^2\cos\alpha\right)}\end{array}\right]/12\xi\kappa\sigma_c x^2 \\ \Delta=h-\frac{h^2\sigma_t\sin\alpha+\sqrt{h^2\sigma_t^{\,2}\sin^2\alpha-48h^2\xi\kappa\sigma_c\sigma_t\left(hx\sin\alpha-x^2\cos\alpha\right)}}{12\xi\kappa\sigma_c x} \end{cases} \tag{25}$$

The angle of rotation and settlement changed with dip angle, which is in the range [20, 70], and the relationship is displayed in Fig. 10. The angle of rotation is positively correlated with the dip angle, indicating that it increases with the dip angle. Equation (25) yields the hinged rock block Δ's settlement. When the settlement of the hinged area of the fractured rock block exceeds Δ, rotatory instability takes place in the roof, and the larger is the dip angle, the more likely is this failure.

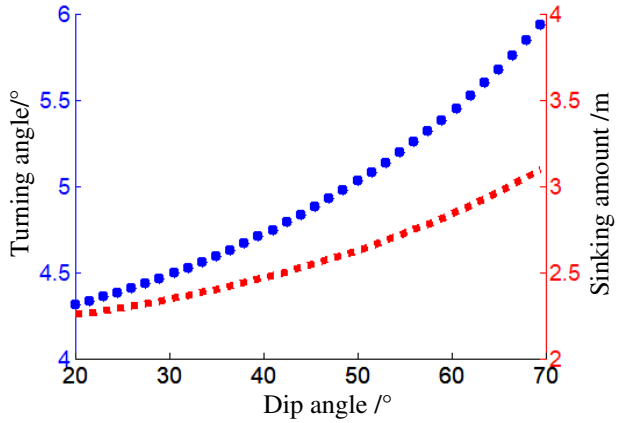

Fig. 10. Relationship between the angle of rotation θ and dip angle α

When the dip angle is constant, the relationships between the angle of rotation and thickness of the main roof, as well as the length of the rock block take the form, as shown in Fig. 11, where 2m<h<5m and 10m< x <30m.

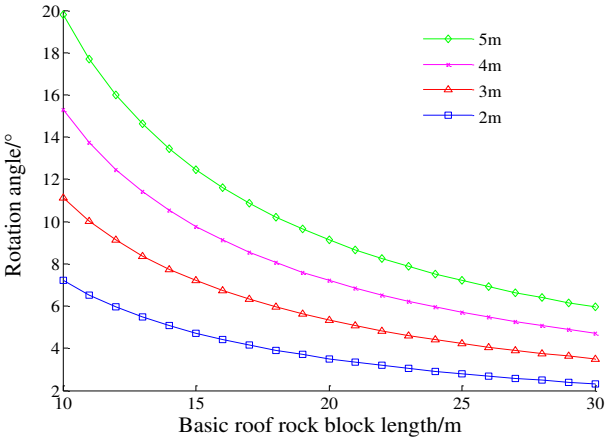

Fig. 11. Relationship between the angle of rotation θ, h, and x

It can be seen from Fig. 11 that the angle of rotation θ grows with an increase of h and x by 1.4~4.3°/m and 0.25~0.69°/m, respectively. It shows that a change in thickness has a larger impact on the hinged structure. When the rotation angle reaches its minimum value depending on the allowable deformation, the deformation instability occurs (He et al. 2020; Ju et al. 2018). The rotation angle's magnitude reflects the differences of overburden rock structure and its stability, thus exerting a significant effect on the support (Xie et al. 2020).

5. Analysis of the support stability

Hydraulic supports are critical in protecting the roof and the dynamic mechanical environment where surrounding rocks impact and constrain each other (Yang et al. 2019; Luo et al. 2019). The load magnitude, direction, and point of application to the support vary with the roof kinematic state changes. Therefore, determining the critical work resistance of support can ensure the particular mining requirements (Yang et al. 2018).

The mechanical model of a single inclined support is shown in Fig. 13, where the x-axis is upward positive and coincides with the workface dip, the y-axis is upward positive and normal to the x-axis, b and h are the support width and height, respectively, h1 is the height of the support center of gravity, x_1 is the point of application of the normal load to the roof, x_2 is the point of application of the normal load resultant to the floor, G is the support weight, P is the normal load of the roof acting on the support (support work resistance), f_1 is the tangential load of the roof acting on the support (friction between roof and support), F_N is the floor tangential load on the support, f_2 is the tangential load of the floor on the support (friction between support and floor), P_{i-1} and P_{i+1} are forces acting between two adjacent supports. During mining in SDCS, forces between adjacent supports are much smaller than friction between support and roof or floor, so forces between adjacent supports are assumed to be the same. The mechanical response of the support in the critical instability state was analyzed in detail.

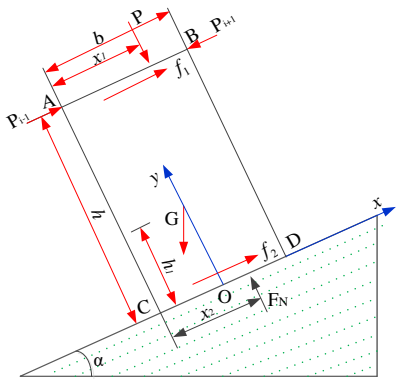

Fig. 12. Mechanical model of a single inclined support

The critical work resistance of the support can be determined when the roof and floor are stable. To avoid

sliding instability, the anti-sliding force should exceed the sliding force in support, which means

$$f_1 + f_2 \geq G\sin\alpha \tag{26}$$

Under the critical sliding instability state, the coefficients of friction between the roof, floor, and support can be expressed as

$$f_1 = \mu_1 P \tag{27}$$

$$f_2 = \mu_2 (P + G\cos\alpha) \tag{28}$$

According to Eqs. (26)-(28), the critical work resistance of a single support before sliding can be expressed as

$$P_{sl} = \frac{G(\sin\alpha - \mu_2\cos\alpha)}{\mu_1 + \mu_2} \tag{29}$$

To avoid rotatory instability, the anti-rotating moment should exceed the turning moment, which means that

$$\frac{b}{2}G\cos\alpha + Px_1 + f_1 h \geq h_1 G\sin\alpha + F_N x_2 \tag{30}$$

During mining in the workface, the loading characteristics of the support, roof, and floor change with time due to the roof and floor movements. When the support work resistance P is applied to A (x_1=0), the resultant force of normal loads on the floor F_N has a point of application C (x_2=0), the support experiences the worst condition before non-rotatory instability. In this case, Eq. (30) can be reduced to the following form

$$\frac{b}{2}G\cos\alpha + f_1 h \geq h_1 G\sin\alpha \tag{31}$$

According to Eqs. (27)-(31), the critical work resistance for single support before rotating can be expressed as

$$\mathrm{P_{ro}} = \frac{2h_1 G\sin\alpha - bG\cos\alpha}{2h\mu_1} \tag{32}$$

As a case study for the proposed method, the 12124 workface in the Pansidong coal was selected to investigate the impact of the dip angle of coal seam on the critical work resistance of support analyzed via Eqs. (29) and (32).

The 12124 workface in the Pansidong mine is fully-mechanized, with the average dip angle of the coal seam α =40°. A ZZ7200/22/45 covering hydraulic support was adopted in the workface, the support width was 1.5 m, the height of the center of gravity of support h1 = 2.25 m, the gravity of support was 176.4 kN, the coefficients of friction between support and roof/floor were equal ($\mu_1 = \mu_2$ =0.25). The relationship between the critical work resistance of support and the dip angle is shown in Fig. 13, where the dip angle ranges from 20º to 70º. It can be seen from Fig. 13 that before slip and rotation of the support, the critical work resistance of support was positively correlated with the dip angle of coal seam and, under the same dip angle, the critical slip work resistance of support exceeded its critical rotation work resistance.

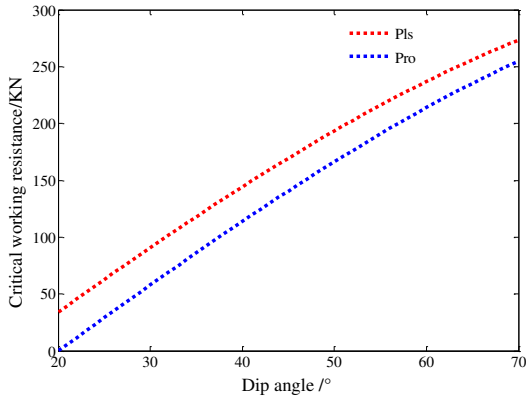

Fig. 13. Relationship between the critical work resistance and dip angle of the coal seam

6. Conclusions

A mechanical model of the main roof under linear load in the SDCS longwall workface was proposed in this study, which made it possible to derive the main roof stresses. The results obtained show that the bottom floor had features of compression at three sides and tension on the middle part, whereas the top floor had tensile stresses at three sides and compressive stress in the middle area. The maximum shear stress $\tau_{\max}$ slightly exceeded the middle of workface and occurred periodically during the workface advance.

The main principal stresses $\sigma_{\max}$ and $\sigma_{\min}$ of the roof were nonlinearly correlated with the dip angle. When the dip angle increased in the range 30°~50°, $\sigma_{\max}$ and $\sigma_{\min}$ rapidly dropped; when the dip angle increases in the range 50°~60°, they gradually become stable. The same variations of the dip corresponded to the same variation rates of $\sigma_{\max}$ and $\sigma_{\min}$.

The mechanical model of the first-fracture rock block in the workface was established, based on which the effects of the dip angle of coal seam on the rock block instability were analyzed. The hinged rock block's anti-slip capacity was improved with an increase in dip

angle, making the slip instability unlikely to occur. The critical dip angle of the fractured rock block was 57° when instability occurred. The possibility of slip instability of a fractured rock block workface increased as the thickness of the main roof and length of the rock block increased.

The critical work resistance of a support under non-sliding and non-rotating conditions was positively correlated with the coal seam's dip angle. The critical work resistance under sliding condition exceeded that under rotating condition at the same dip angles of the coal seam.

Acknowledgments We acknowledge the financial support for this work provided by the China National Key Research and Development Program (2019YFC1904304) and the National Natural Science Foundation of China (grant No. 51634007).

References

Das A J, Mandal P K, Bhattacharjee R (2017) Evaluation of Stability of underground workings for exploitation of an inclined coal seam by the ubiquitous joint model. International Journal of Rock Mechanics and Mining Sciences 2017: 101-114.

Cui F, Lei ZY, Chen JQ, Chang B, Yang YB, Li CL (2019) Research on Reducing Mining-Induced Disasters by Filling in Steeply Inclined Thick Coal Seams. Sustainability 11(20).

He SQ, Song DZ, He XQ, Chen JQ, Ren t, Li ZL, Qiu LM (2020) Coupled mechanism of compression and prying-induced rock burst in steeply inclined coal seams and principles for its prevention. Tunnelling and Underground Space Technology 98.

Hu ZQ (2018) Special issue on land reclamation in ecological fragile areas. International Journal of Coal Science & Technology 5(1):1-2.

Sun J, Wang LG, Zhao GM (2019) Stress Distribution and Failure Characteristics for Workface Floor of a Tilted Coal Seam. KSCE Journal of Civil Engineering. 23(9), 3793-3806.

Jiang JQ, Zhang PP, Nie LS, Li HX, Wang WD (2014) Fracture law and dynamic response analysis of high hard and thick rock formations. Chinese Journal of Rock Mechanics and Engineering 33(07):1366-1374.

Wang JA, Jiao JL (2016) Criteria of support stability in mining of steeply inclined thick coal seam. International Journal of Rock Mechanics and Mining Sciences, 2016: 100(82): 22-35.

Ju Y, Sun HF, Xing MX , Wang XF Zheng JT (2018) Numerical analysis of the failure process of soil–rock mixtures through computed tomography and PFC3D models. International Journal of Coal Science & Technology 5(2): 126–141.

Kang JR, Wang JZ. (2002) Analysis of mechanical model of mining overburden and fracture failure conditions. Journal of China Coal Society (01):16-20.

Luo SH, Wu YP, Xie PS, Wang HW, Zhang H (2019) Mechanical analysis of support stability in longwall mining with large inclined seam strike. Journal of China Coal Society 44(09): 2664-2672.

Shan PF, Lai XP (2020) An associated evaluation methodology of initial stress level of coal-rock masses in steeply inclined coal seams, Urumchi coal field, China. Engineering Computations 37(06).

Hu SX, Ma LQ, Guo JS , Yang PJ (2017) Support-surrounding rock relationship and top-coal movement laws in large dip angle fully-mechanized caving face. International Journal of Mining Science and Technology 28(03): 533-539.

Shi F, Wang HT, Shu C (2018) Similar simulation test research on the influence of coal seam dip on the deformation law of mining overburden. Journal of Chongqing University 41(12): 36-45.

Tu HS, Tu SH, Zhu DF, Hao, DY, Miao, KJ (2019) Force-Fracture Characteristics of the Roof above Goaf in a Steep Coal Seam: A Case Study of Xintie Coal Mine. Geofluids 2019:1-11.

Wang BN, Dang FN, Chao W, Miao YP, Li Ju, Chen F (2019) Surrounding rock deformation and stress evolution in pre-driven longwall recovery rooms at the end of mining stage. International Journal of Coal Science & Technology 6(4): 536-546.

Wang JC, Wang ZH (2015a) Research on the stability of the basic roof structure under the initial pressure in the shallow-buried thin bedrock high-strength mining face. Journal of Mining and Safety Engineering 32(02): 175-181.

Wang XF,Gao MZ (2015b) Mechanical model analysis of roof breaking mechanism in variable length working face. Journal of China University of Mining & Technology 44(01):36-45.

Wu YP, Liu KZ, Yun DF, Xie PS Wang HW (2014) Research progress in safe and efficient mining technology for large inclined coal seams. Journal of China Coal Society 39(8):1611-1618.

Wu YP, Xie PS, Wang HW, Ren SG (2010) Surface oblique masonry structure of overlying strata in mining of large dip angle coal seam. Journal of China Coal Society 35(08):1252-1256.

Xie GX , Chang JC , Yang K (2009) Investigations into stress shell characteristics of surrounding rock in fully mechanized top-coal caving face. International Journal of Rock Mechanics and Mining ences 46(1):172-181.

Xie PS , Zhang YY , Luo SH , Duan JJ (2020) Instability Mechanism of a Multi-Layer Gangue Roof and Determination of Support Resistance Under Inclination and Gravity. Mining Metallurgy & Exploration, 37(8):1487–1498.

Xie SR, Gao MM, Chen DD, Yue SS, Pan H, Zeng JC, Suo HX (2019) Study on the distribution and evolution of the spherical stress shell in the backfill mining stope[J]. Journal of Mining and Safety Engineering 36(01):16-23.

Yang K, Chi XL, Liu S (2018) Mechanism and control of hydraulic support instability in fully mechanized mining face in large inclined seam. Journal of China Coal Society 43(07): 1821-1828.

Yang K, He X, Dou LT, Liu WJ, Sun L, Ye HS (2015) Experimental investigation into stress-relief char-acteristics with upward large height and upward mining under hard thick roof. International Journal of Coal Science & Technology 2(1):91－96.

Yang K, Liu S, Tang CA, Wei Z, Chi XL (2019) The mechanism and prevention of coal wall slicing in long-distance protected seams across coal groups with multiple key layers. Journal of China Coal Society 44(09):2611-2621.

Yang PJ, He Ye, Guo WB (2013) Disaster mechanism and prevention and control measures of huge thick hard magmatic rock overlying stope. Journal of China Coal Society 38(12): 2106-2112.

Ye Q, Wang WJ, Wang G, Jia ZZ (2017) Numerical simulation on tendency mining fracture evolution characteristics of overlying strata and coal seams above working face with large inclination angle and mining depth. Arabian journal of geosciences 10(4):82.

Zhang S, Wang XF, Fan GW, Zhang DS, Cui JB (2018) Pillar size optimization design of isolated island panel gob-side entry driving in deep inclined coal seam—case study of Pingmei No. 6 coal seam. Journal of Geophysics and Engineering 15(3): 816-828.

Zhang T, Yuan L, Zhao YX, Hao XJ (2015) The geometric characteristics of the fracture zone in deep stope of thin bedrock and thick loose layer and the effect of mining pressure distribution on working face. Journal of China Coal Society 40(10): 2260- 2268.

Zhang YD, Cheng JY, Wang XX, Feng ZJ, Ji M (2010) Thin plate model analysis of roof fracture in large dip angle upward (pitching) stope. Journal of mining and safety engineering 27 (04): 487-493.

Zhao YX, Wang XZ, Zhou JL, Li QS, Zhang C (2019) The influence of the basic top thickness-span ratio of fully mechanized mining face on its initial fracture instability. Journal of China Coal Society 44(01):94-104.

Zhou JL, Huang QX (2019) Structural stability analysis of the roof key layer of the shallow-buried large mining height working face. Chinese Journal of Rock Mechanics and Engineering 38(07):1396-1407.

Figures

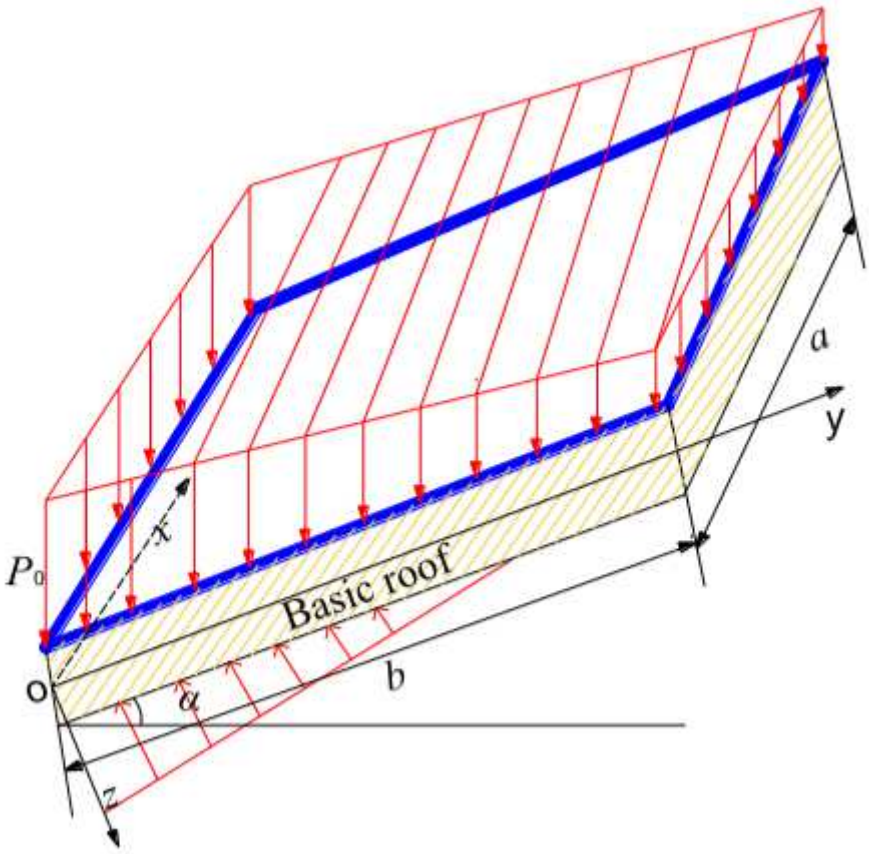

Figure 1

Mechanical model of the main roof in SDCS

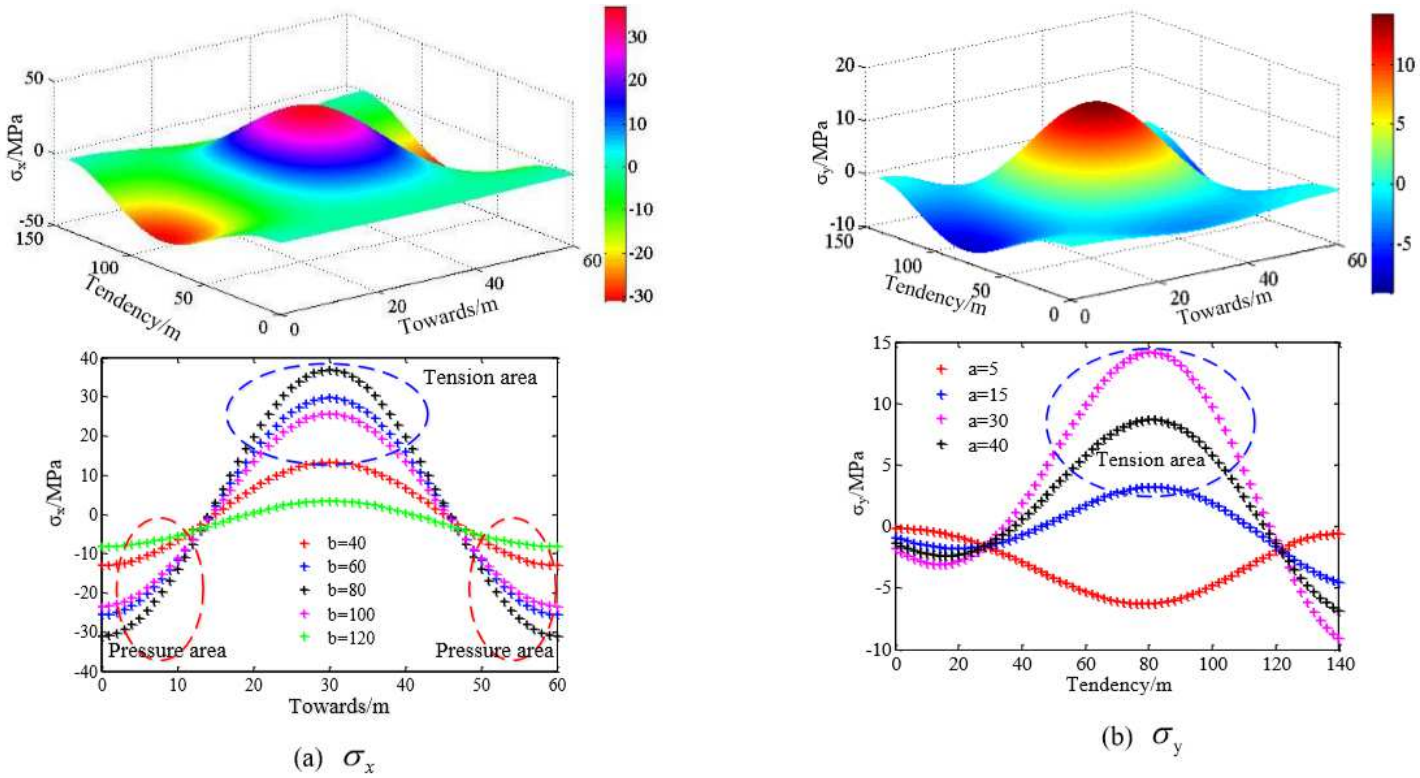

Figure 2

Characteristics in the bottom floor of the thin plate

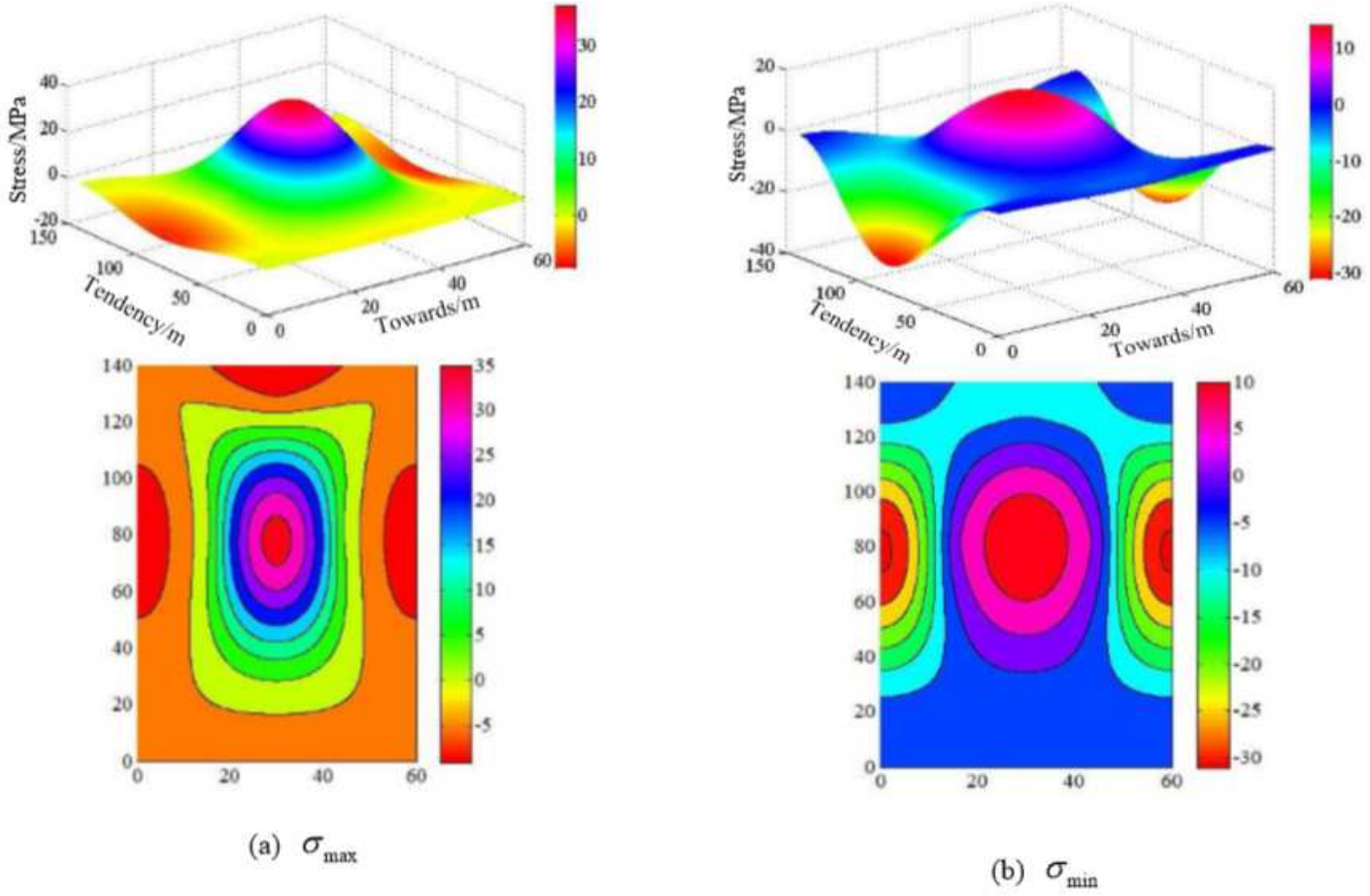

Figure 3

Neophogram of the principal stress in the main roof

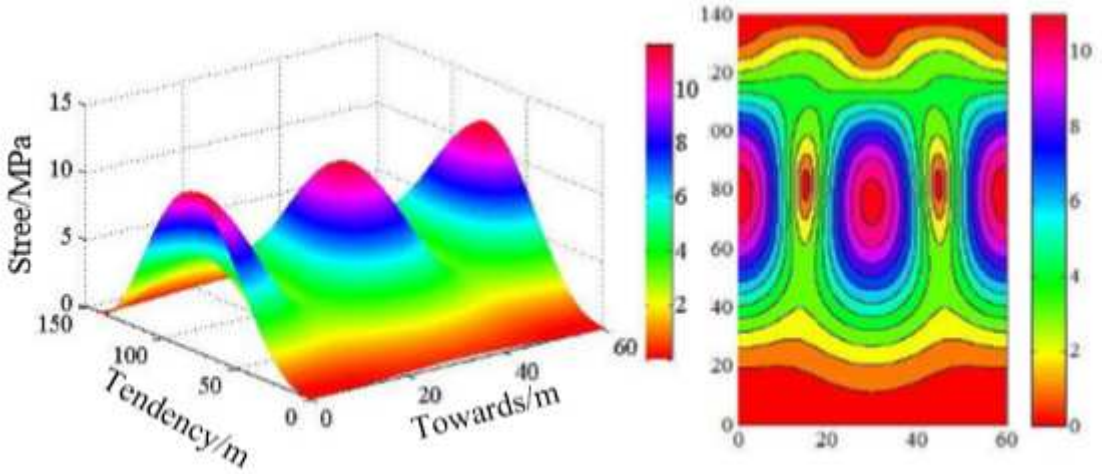

Figure 4

Neophogram of maximum shear stress of the main roof

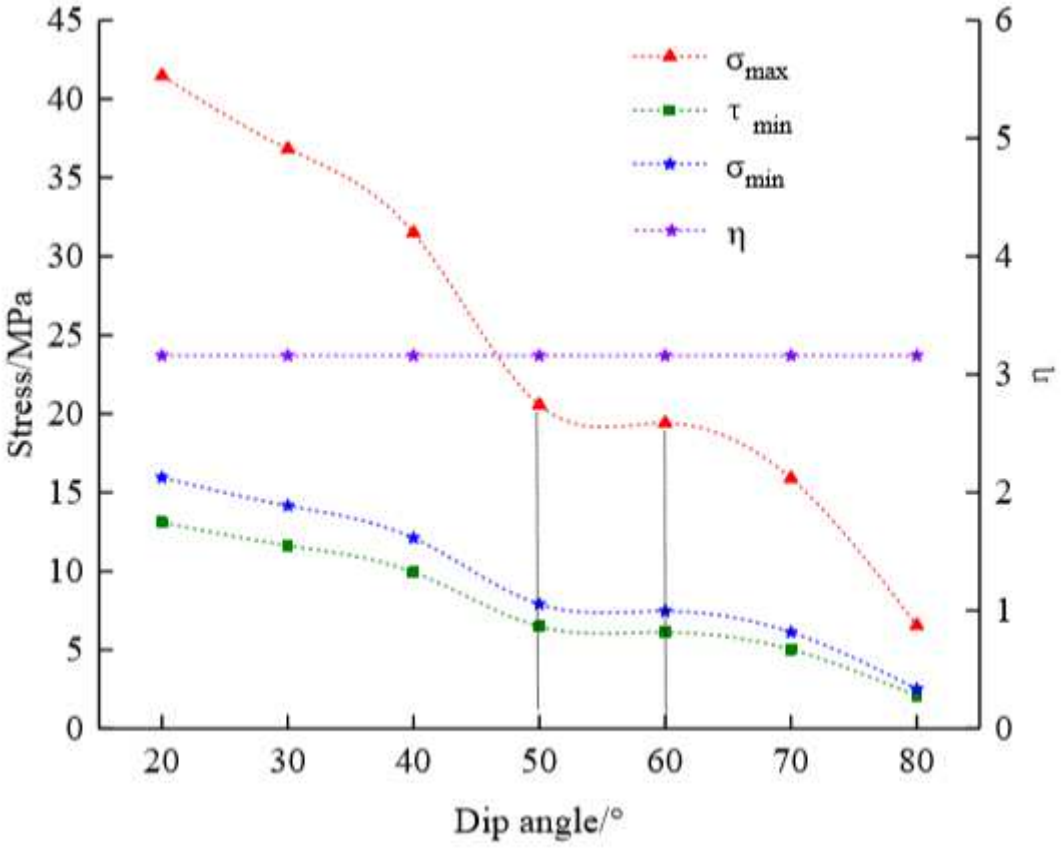

Figure 5

Relationship between stresses in the thin stratum and the dip angle

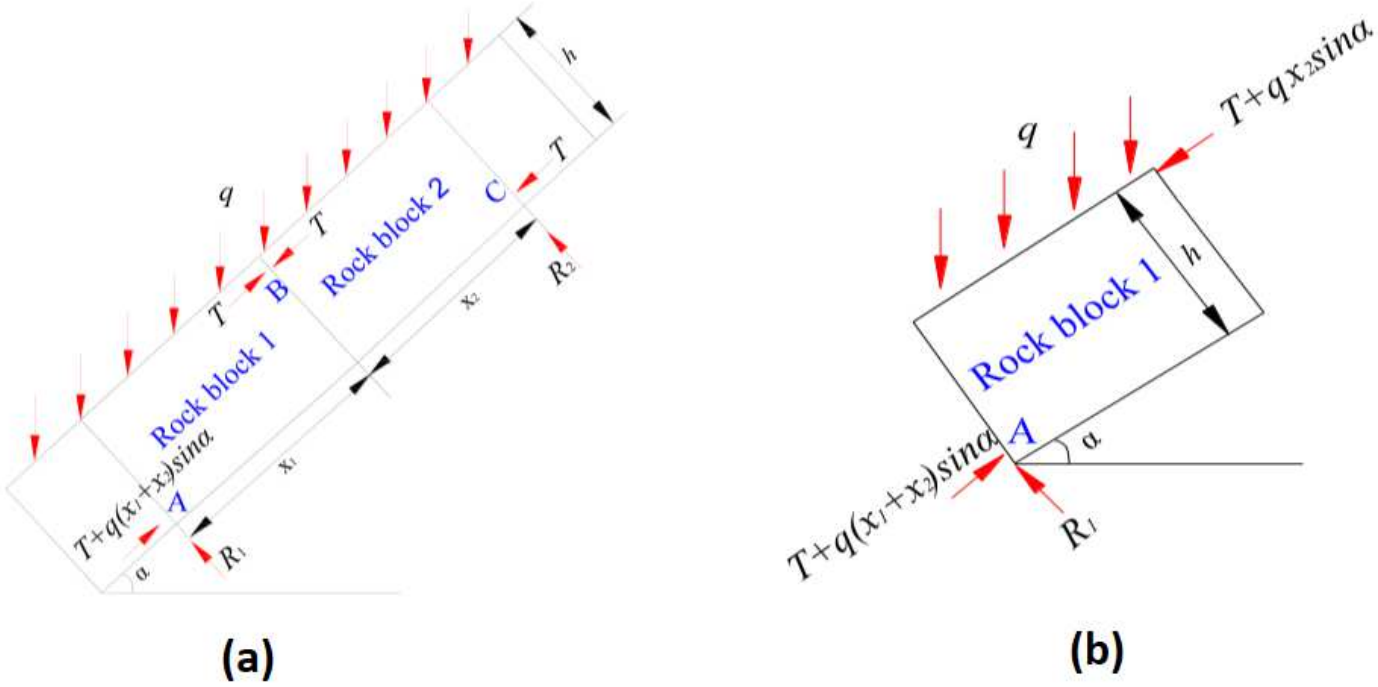

Figure 6

Mechanical model of the inclined fractured rock block □a□stress characteristics of the whole model (b) stress characteristics of the rock block 1

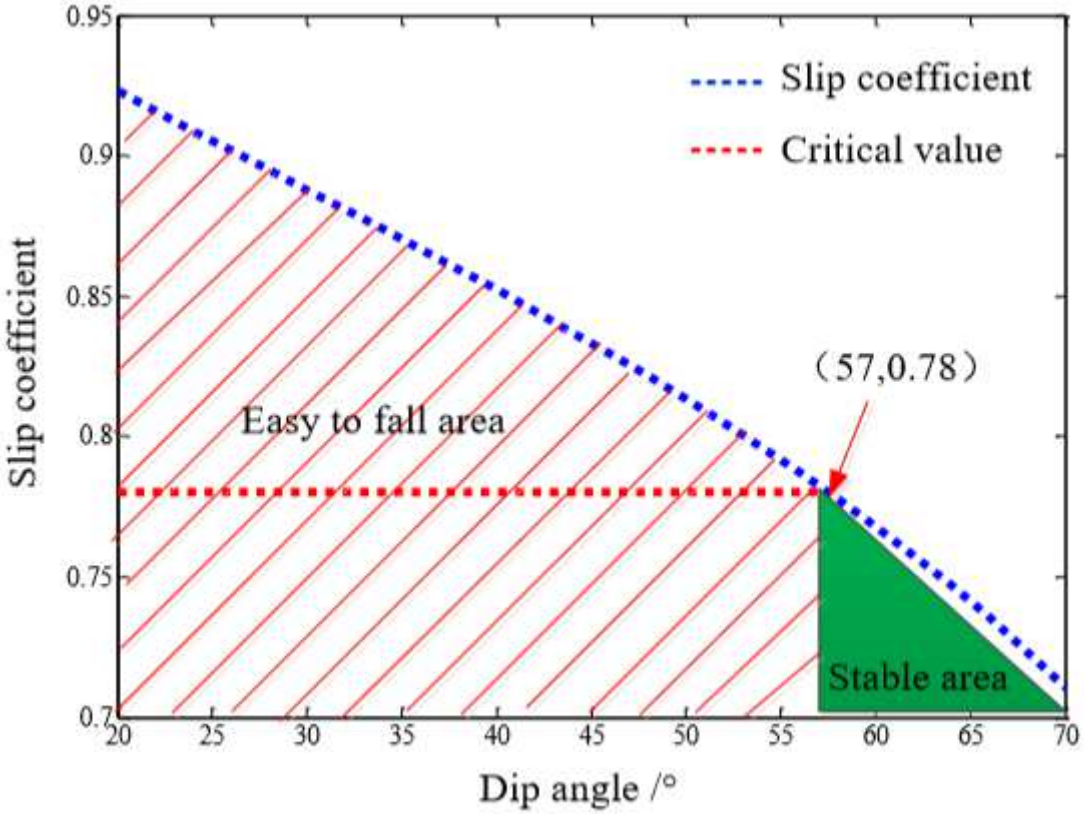

Figure 7

Relationship between slip coefficient λ and dip angle α

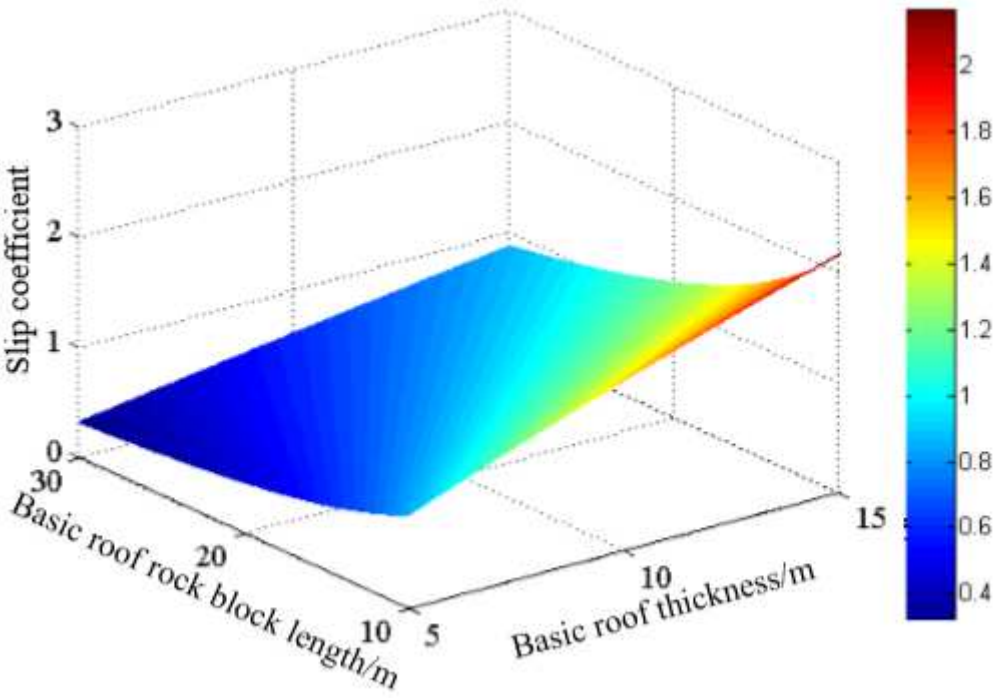

Figure 8

Relationship between slip coefficient λ, main roof thickness h , and length x

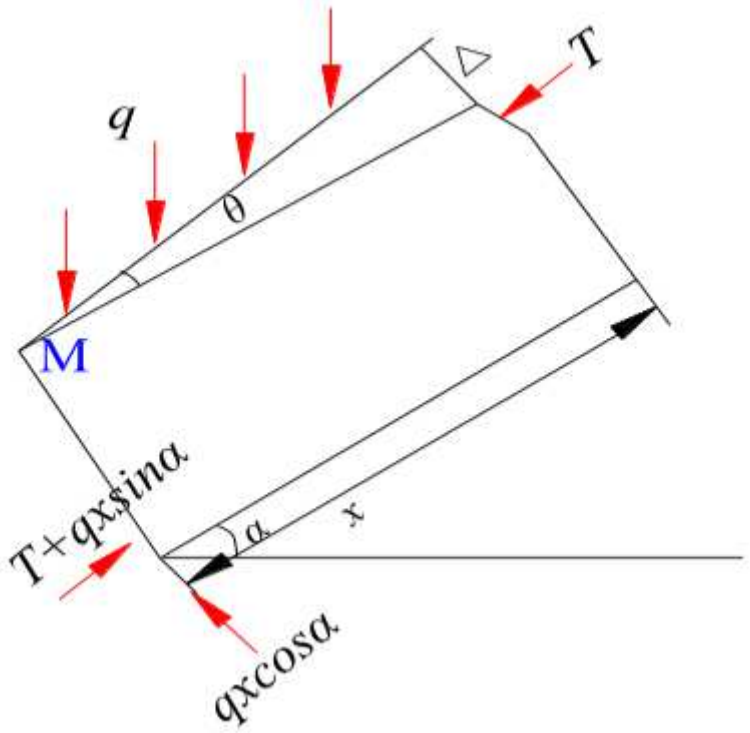

Figure 9

Rotatory instability mechanical model of fractured rock block

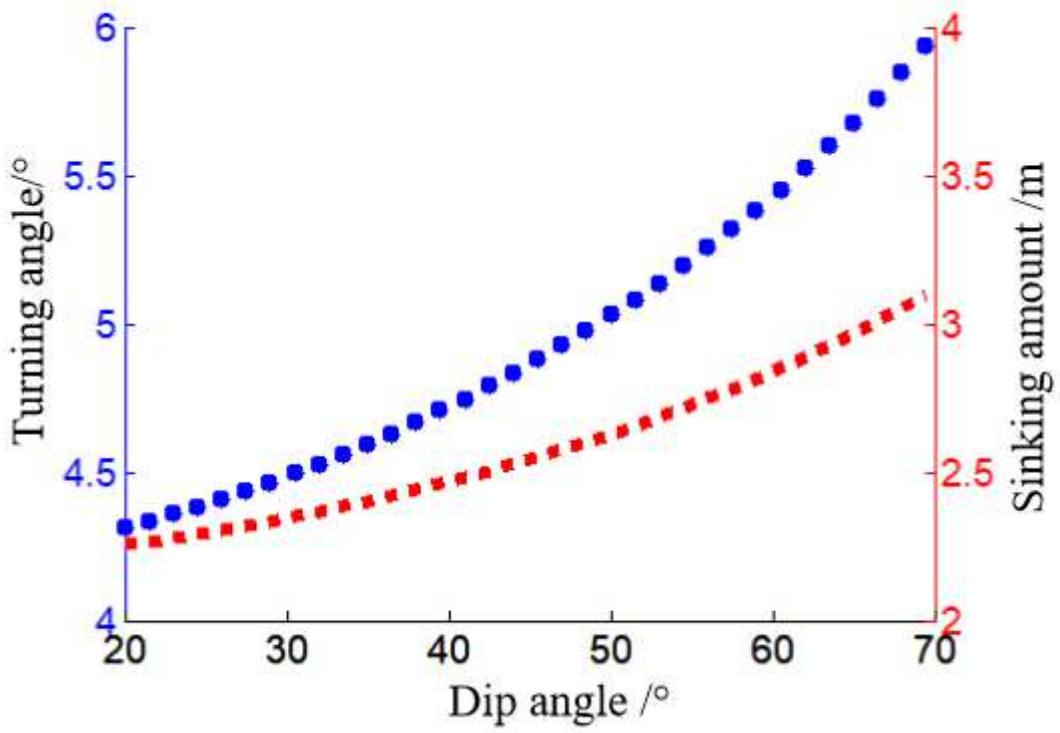

Figure 10

Relationship between the angle of rotation θ and dip angle α

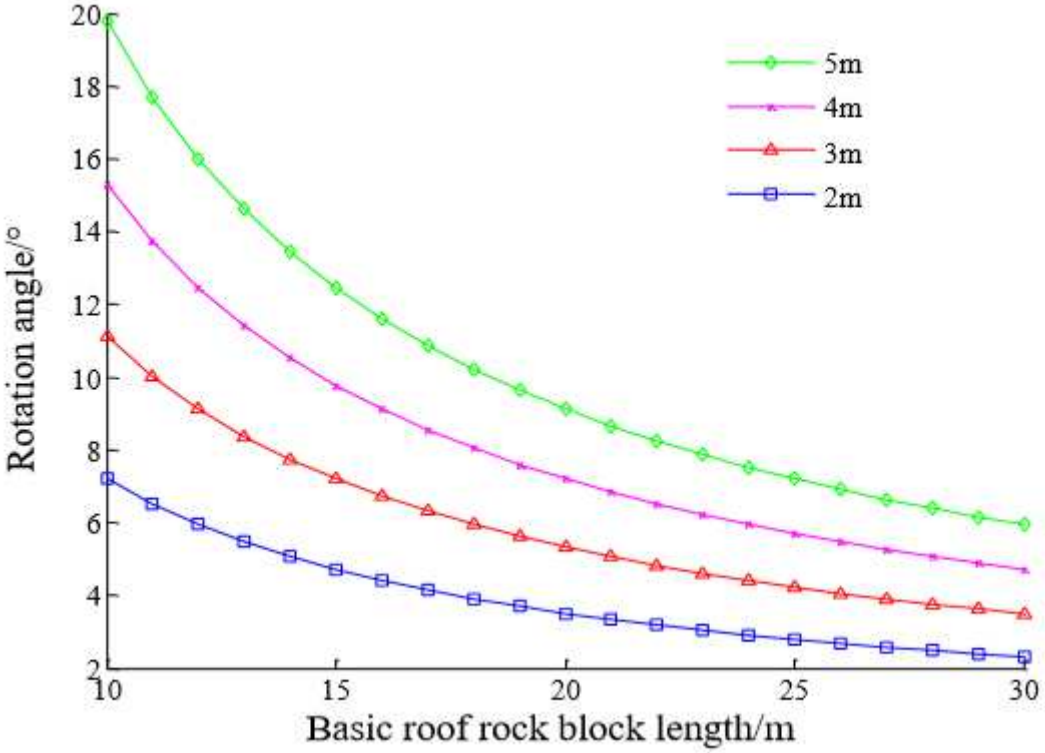

Figure 11

Relationship between the angle of rotation θ, h, and x

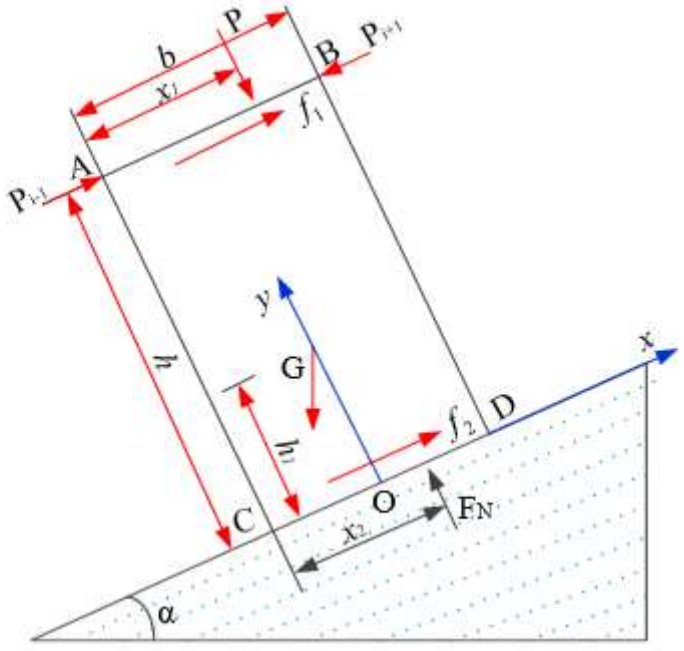

Figure 12

Mechanical model of a single inclined support

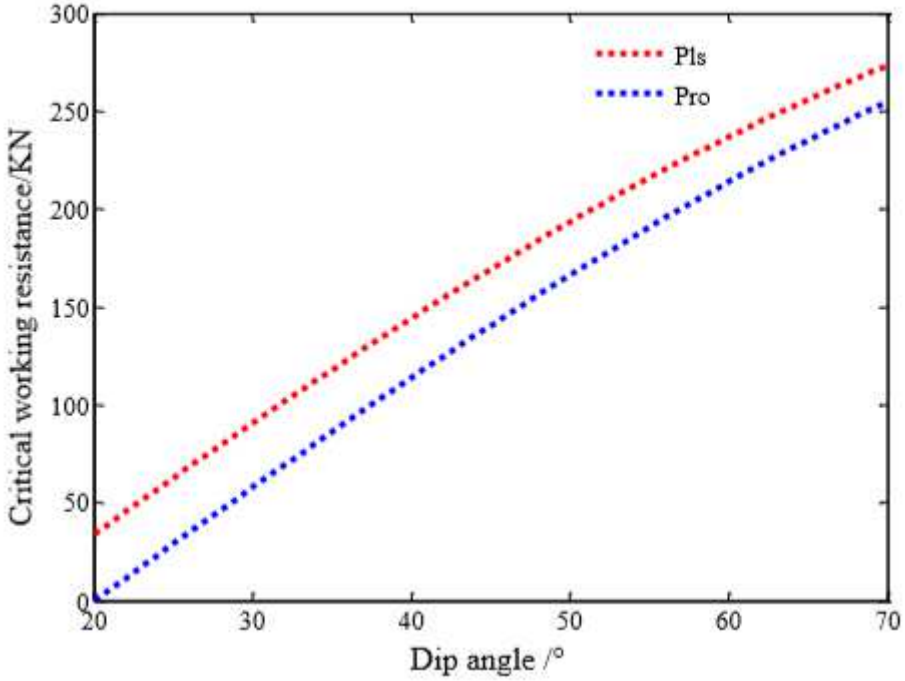

Figure 13

Relationship between the critical work resistance and dip angle of the coal seam